Graphene nanoribbons subjected to axial stress

M. Neek-Amal[1] and F. M. Peeters[2]
[1]*Department of Physics, Shahid Rajaei University, Lavizan, Tehran 16785-136, Iran*
[2]*Departement Fysica, Universiteit Antwerpen, Groenenborgerlaan 171, B-2020 Antwerpen, Belgium*
(Received 26 April 2010; revised manuscript received 1 July 2010; published 20 August 2010)

Atomistic simulations are used to study the bending of rectangular graphene nanoribbons subjected to axial stress both for free boundary and supported boundary conditions. The shapes of the deformations of the buckled graphene nanoribbons, for small values of the stress, are sine waves where the number of nodal lines depend on the longitudinal size of the system and the applied boundary condition. The buckling strain for the supported boundary condition is found to be independent of the longitudinal size and estimated to be 0.86%. From a calculation of the free energy at finite temperature we find that the equilibrium projected two-dimensional area of the graphene nanoribbon is less than the area of a flat sheet. At the optimum length the boundary strain for the supported boundary condition is 0.48%.

DOI: 10.1103/PhysRevB.82.085432 PACS number(s): 62.25.−g

I. INTRODUCTION

Graphene is a newly discovered almost flat one-atom-thick layer of carbon atoms which exhibits unique electronic properties and unusual mechanical properties.[1,2] Recent experiments showed that compressed rectangular monolayer graphene on a substrate with size 30×100 μm^2 is buckled at about 0.7% strain.[3] Moreover tensional strain in monolayer graphene affects the electronic properties of graphene. The strain can generate a bulk spectral gap in the absence of electron-electron interactions as was found within linear elasticity theory and a tight-binding approach.[4] Different morphological patterns of carbon nanostructures subjected to external stress were obtained by using atomistic simulations.[5] Furthermore, atomistic simulations showed that the Young modulus and the fracture strength decrease only weakly with the width of the graphene nanoribbon.[6]

In this paper we study the deformations and the stability of rectangular monolayer graphene nanoribbons (GNRs) subjected to axial stress using atomistic simulations and the Jarzynski theorem to calculate the free energy.[7] Recently, Colonna *et al.* applied the free-energy integration-based method to explain the melting properties of graphite.[8] We will compare the obtained critical buckling force with the one predicted by elasticity theory. We found several longitudinal deformation modes and predict that the axial buckling boundary strain is independent of the size in the case of laterally supported GNRs. Moreover, from a calculation of the free energy, uncompressed GNR is thermodynamically less stable than the GNR at the buckling threshold. But the buckled state is less stable than the GNR at its optimum length.

This paper is organized as follows. In Sec. II we introduce the atomistic model and the simulation method. Section III contains a discussion of the elasticity theory predictions for both free boundary condition and laterally supported boundary condition. We also give the buckling thresholds and the obtained deformations and compare our results to those from elasticity theory. Results for the Young's modulus and prestresses are presented and compared to available experimental results. The stability of buckled GNRs are studied in the last part of Sec. III. In Sec. IV we will conclude the paper.

II. METHOD AND MODEL

Classical atomistic molecular-dynamics (MD) simulations are employed to simulate compressed GNRs using Brenner's bond-order potential.[9] Our system is a rectangular GNR with dimensions $a\times b$, in x and y directions with armchair and zigzag edges, respectively. For simplicity we set the lateral dimension $b=10n_y\sqrt{3}a_0$, where $a_0=0.142$ nm, $n_y=3,4$, and the longitudinal dimension $a=30n_xa_0$ with $n_x=2,3,\ldots,10$. In Fig. 1 we depict a schematic model for a GNR under axial strain with free boundary condition (at $y=0$ and $y=b$) and list all relevant variables describing GNR under axial strain. Note that n_x and n_y are two integer numbers that are related to the number of atoms in the armchair and zigzag directions, respectively. The corresponding values for length and width of GNRs can be found in Table I.

Initially the coordinates of all atoms are put in a flat surface of a honeycomb lattice with nearest-neighbor distance equal to a_0 and the initial velocities were extracted from a Maxwell-Boltzman distribution at the given temperature. Before starting the compression, the system is equilibrated during 50 ps (100.000 time steps). Compressing direction is always x and two rows of atoms in both right and left edges, $x=0$ and $x=a$, are fixed during the compression steps ($\delta x=0.04$ Å) with the rate $\mu=1.6$ m/s. The boundary axial strain after t compression steps is

$$\epsilon_x = t\epsilon_0, \quad \epsilon_0 = 2\delta x/(30a_0n_x), \tag{1}$$

where $\epsilon_0=\frac{0.188}{n_x}\%$ is the strain after a single compression step. After each compression step, we wait 2.5 ps to allow the system to relax. For the edges at $y=0$ and $y=b$, we used the supported boundary condition and the free boundary condition. We simulated the system at room temperature and employed a Nosé-Hoover thermostat.

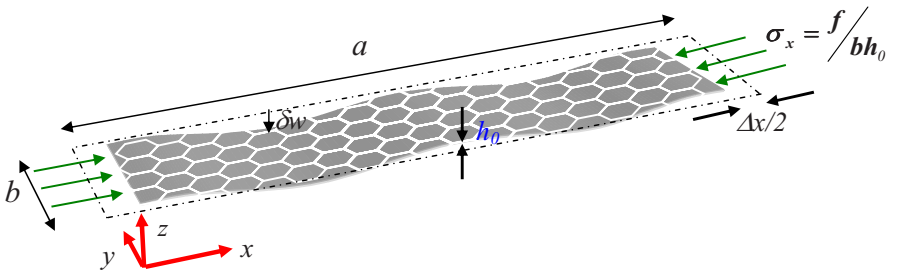

h_0, h	Thickness of GNR, Out of plane of GNRs atom
ε_0, ε_x, ε_c, ε_m	Strain in each step, Total strain, Critical strain, Strain at optimum length
σ_0, σ_x, σ_c, σ_m	Pre-stress, Total stress, Critical stress, Stress at optimum length
E, ν, D	Young's modulus, Poisson's ratio, Flexural rigidity
f, f_c, f_{mn}, f'_{mn}	Force, Critical force, Critical force from elasticity theory for h_0=0.1 nm and $h_0=a_0$
n,m	Sinusoidal modes in x and y direction
t, μ	Compression step in simulation, Compression rate
ΔW, ΔF	Difference of total work and free energy between initial and strained states

FIG. 1. (Color online) Schematic model for a plate under axial strain with free boundary condition (a model for elasticity theory), dashed-dotted rectangle is the initial noncompressed plane. We list all relevant variables describing the GNR.

III. BUCKLING GRAPHENE NANORIBBONS AND COMPARISON WITH ELASTICITY THEORY

A. Free boundary condition

For a simple bar with length a, under an axial symmetric load applied at its ends, classical Euler's column equation describes basically the buckling problem.[10] Governing differential equation for the deflection value, δw, becomes the harmonic oscillator equation

$$\delta w'' + \kappa^2 \delta w = 0. \tag{2}$$

Here $\kappa^2 = f_c/P$, where f_c is the buckling force (or critical force), P is a parameter which is related to the Young's modulus and the moment of inertia of the rod cross-sectional axis that is perpendicular to the buckling plane. The solution is $\delta w = A\sin(\kappa x) + B\cos(\kappa x)$. For the boundary condition with zero deflection at the ends, we have $\delta w = A\sin(\frac{n\pi}{a}x)$ which are sine waves. Substituting $\kappa = \frac{n\pi}{a}$ yields the buckling force

$$f_c = \frac{n^2\pi^2 P}{a^2} \quad (n = 1,2,\ldots). \tag{3}$$

The buckling stress can be written as $\sigma_c = \frac{f_c}{S}$, where S is the area of the cross section of the bar. If the bar is thin enough or long enough buckling can happen elastically independent of the type of material.[10]

The shape of the lowest mode (n=1), after and close to the buckling threshold, is a half sine wave. Higher modes are possible only if the column is physically constrained from buckling into the lower modes by supporting mid points.[10]

For GNRs under axial compression with free boundary condition we focused on the system with n_y=3. After many compression steps GNRs starts to buckle, but the shape of the deformed GNRs depends on their size. Figure 2(a) shows some snapshots for the deformed GNRs with various sizes when Δx=0.768 nm, i.e., beyond the buckling threshold. We will discuss on the obtained shapes later. By measuring the buckling threshold, we find the forces which cause a sudden change in the shape of GNRs. This threshold is found from a direct visualization of the nanoribbon and in addition from the sudden increase in the average out-of-plane displacement of the GNR atoms ($\langle h^2\rangle$). The variation in $\langle h^2\rangle$ versus ϵ_x for systems with n_x=3 and 10 are shown in Fig. 2(b). The longer GNRs have a smaller buckling strain, $\epsilon_c \simeq 1.2\%$, 2.1% for n_x=10, 3, respectively.

On the other hand, as can be seen from the simulation snapshots in Fig. 2(a), even for large samples, in contrast to the large deformations along the x direction, the deformations along the y direction for each x value and also deformations at the boundaries (y=0 and y=b) for each x value are negligible. Therefore the rod assumption for GNRs under axial strain is a good approximation. Now, considering the GNR as a rod with length a and estimating the buckling forces, allow us to calculate the variation f_c versus GNR length, i.e., a. Furthermore, note that throughout the present paper, we calculate the force per width. Since for $n_x \leq 5$ we found only deformations with n=1 in the beginning of the

TABLE I. Length a and width b of GNRs which are related to the integer numbers n_x and n_y through $b = 10n_y\sqrt{3}a_0$ and $a = 30n_x a_0$, where a_0=0.142 nm.

n_x	2	3	4	5	6	7	8	9	10	n_y	3	4
a (Å)	85.2	127.8	170.4	213	255.6	298.2	340.8	383.4	426	b (Å)	98.38	122.96

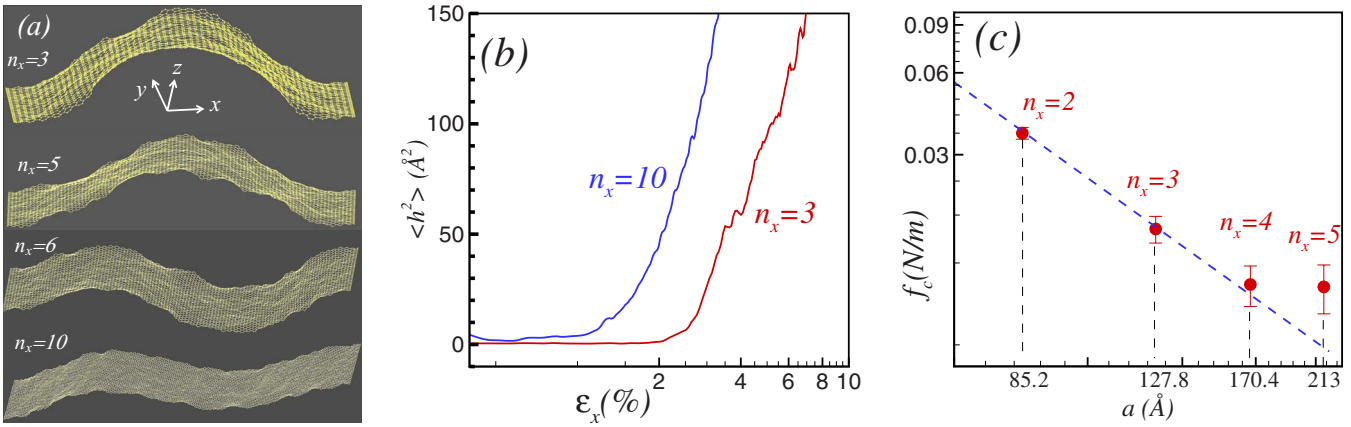

FIG. 2. (Color online) (a) Buckled graphene nanoribbons for four different length n_x. Here Δx=0.768 nm. (b) Variation in the out-of-plane displacement in log scale for GNRs with two different lengths versus strain. (c) Symbols are the calculated buckling force in log-log scale and dashed line is the curve $f_c=\frac{\pi^2 P}{a^2}$.

buckling, hence using Eq. (3) is justified. Figure 2(c) shows the variation in the critical load versus a in log-log scale where the dots are from our simulation results and the dashed line is $\frac{\pi^2 P}{a^2}$. Here we used Eq. (3) for the buckling force, but, since our system is not a rod, the definition of an axial moment of inertia is not meaningful. Therefore, we define an effective bending constant for GNRs, i.e., P. Taking the parameter P as a fitting parameter, we found $P \simeq 0.56$ eV. The corresponding number for a covalent carbon bond is 4.0 eV.[11] Clearly the bending stiffness for a single covalent C-C bond should be much larger than a long rod made of GNR.

Here we discuss the shapes of the deformation. As we mentioned above, at the start of the buckling the shape of systems with $n_x \leq 5$ is found to be almost the same as for a buckled rod width $n=1$, which is similar to half sine waves. Note that we should neglect the few rows of atoms at both ends which are fixed during the compression resulting in flat ends (see Sec. II). By continuing the compression up to the time 0.5 ns, GNRs acquire a parabolic shape. The top two pictures in Fig. 2(a) show two snapshots of the obtained deformations after the buckling threshold when $\epsilon_x=2\times\frac{0.34}{n_x}$ =6%,3.6% for n_x=3,5, respectively. For a fixed reduction in the length, Δx, the system with larger n_x has a smaller amplitude, i.e., 2.609 nm and 3.412 nm for n_x=5 and n_x=3, respectively. For larger GNRs ($n_x \geq 6$), i.e., a is larger than 21.3 nm, the deformations [two bottom figures in Fig. 2(a)] first show the next higher mode with $n \simeq 2$ and after a longer simulation time (depending on the size) they transit slowly to the mode $n=1$. When the length of GNRs exceeds almost 22 nm, half of this size is comparable to the chrematistic length of graphene, i.e., 8–10 nm.[12] Since the chrematistic length is a measure of the range over which deformations in one region of graphene are correlated with those in another region, so the applied boundary stresses on the edges do not affect the system beyond this characteristic length and in the beginning of the buckling we expect the $n \simeq 2$ mode. For GNR with $n_x \geq 6$ we did not find a simple relation between the critical buckling force and the length. For larger systems ($n_x > 10$) the deformations are no longer sine waves at least during our simulations time.

Before ending this section, we calculate the stress-strain curve. Before the buckling threshold, we found a linear relation between stress and strain, i.e., $\sigma_x=E\epsilon_x+\sigma_0$, where σ_0 is the prestress in the system.[1] The linear relation is valid for small strains.[1,13] In our simulations, when the GNRs are not flat and thus not compressed, they are not in equilibrium and some boundary tension exist, i.e., prestress.[1] For instance, when n_x=8 we calculate the applied stress on the right-hand side edge using $\frac{f}{bh_0}$ [by using the thickness of graphene equal to h_0=0.1 nm (Ref. 14)] and we show the obtained stress-strain curve in Fig. 3. The dashed line is the fitted line. The slope of this line gives us Young's modulus 1.3 ± 0.07 TPa and $\sigma_0=-3.3 \pm 0.2$ GPa (negative sign indicates the direction of compression, i.e., $-x$). For the other GNRs we found Young's modulus in the same range (e.g., $E=1.1 \pm 0.08$ TPa and $\sigma_0=-3.3 \pm 0.2$ GPa for n_x=10, etc.). These numbers are comparable to those found experimentally.[1]

B. Supported boundary condition

For a rectangular plate subjected to the supported boundary condition (when movements at $x=0$, $x=a$, $y=0$, and y

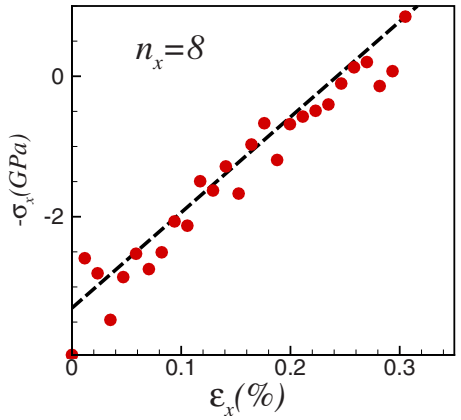

FIG. 3. (Color online) Stress-strain curve for the GNR with n_x =8 under axial stress before the buckling threshold where.

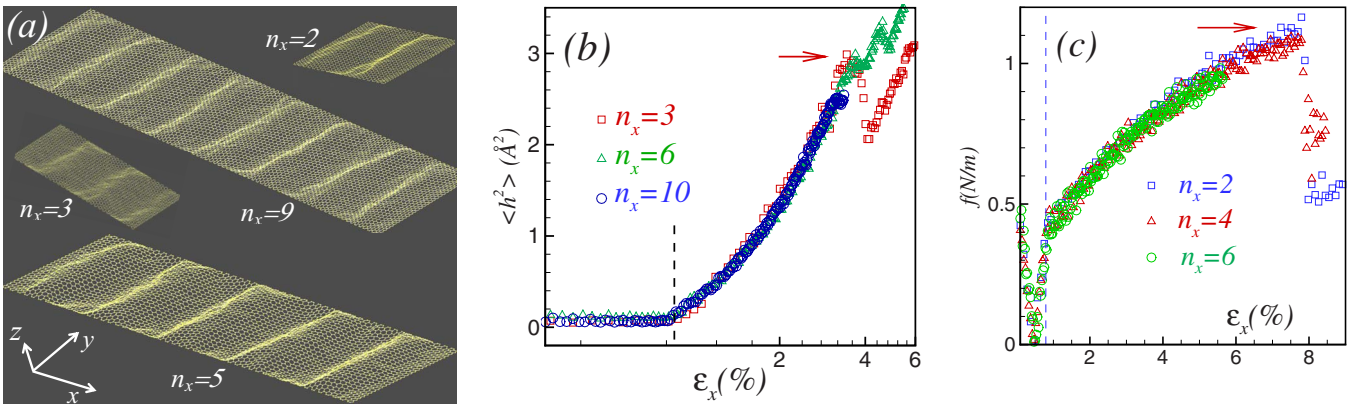

FIG. 4. (Color online) (a) Buckled graphene nanoribbons for four different length subjected to a lateral supported boundary condition. Here applied strains are larger than the buckling strains. (b) Variation in the out-of-plane displacement in log-log scale for GNRs for three different lengths versus strain. (c) Force applied on the boundaries for three different sizes: $n_x=2,4,6$. Horizontal arrow shows the instability point and vertical dashed line shows the buckling point.

$=b$ along y and z directions are not allowed), elasticity theory[10] tells us that the governing equation for the buckled rectangular under uniform compressive axial load per width (f) in the x direction, can be written as

$$D\nabla^4(\delta w) + f(\delta w_{xx}) = 0, \tag{4}$$

where δw is the transverse deflection, δw_{xx} is the corresponding curvature, and $D=Eh_0^3/[12(1-\nu^2)]$ is the flexural rigidity of the plate with thickness h_0 and Young's modulus E. The general solution for the deflection can be written as a double Fourier series

$$\delta w = \sum_{m,n=1}^{\infty} \tilde{w}_{mn} \sin(n\pi x/a)\sin(m\pi y/b), \tag{5}$$

where (m,n) are integers in order to satisfy the supported boundary condition and $\tilde{w}_{mn}$ is the amplitude of each mode (m,n). Including the appropriate strain energy and using Eq. (5), buckling occurs when[10]

$$f_{mn} = \frac{\pi^2 a^2 D}{n^2}\left[\left(\frac{n}{a}\right)^2 + \left(\frac{m}{b}\right)^2\right]^2. \tag{6}$$

Lowest value of f_{mn} with respect to the two discrete variables m,n gives the buckling force, f_c. The minimum buckling force for the considered systems always occurs for $m=1$ and various values of n. It is equivalent to a single half wave in the lateral y direction and various harmonics n in the compression direction, i.e., x.

We performed several atomistic simulations for GNRs under supported boundary condition for different n_x and fixed $n_y=3$. In Fig. 4(a), we depict four typical snapshots for different sizes of the buckled GNRs (where ϵ_x is always larger than the buckling strain, ϵ_c). As can be seen from this figure, those satisfy the condition $m=1$, and by increasing the size of the system, we obtained higher longitudinal modes. Furthermore, higher strains ($\epsilon_x > \epsilon_c$) increase the amplitude of the deformations and increase the number n slightly (usually $n'=n+1,n+2$). Similar to the free boundary condition case, the buckling thresholds, for smaller n_x, are obtained at smaller axial strains. In Table II, we list our calculated buckling forces per width (f_c), buckling strains and the prediction from elasticity theory according to Eq. (6). To calculate f_{mn}, we used $E=340$ N/m^2 and $\nu=0.165$ (Ref. 1) with $h_0 \sim 0.1$ nm, as a typical thickness for GNR. Larger thickness yields a larger f_{mn} so that $h_0=a_0$ yields a better agreement between f_c' and f_{mn}. Note that elasticity theory is not applicable to GNRs under strain[3] for the critical values for force or strains. For instance, although elasticity theory predicts that the very small thickness of graphene yields a zero flexural rigidity but the bond-angle effects on the interatomic interactions of graphene (three body terms in Brenner's potential) gives a nonzero flexural rigidity for graphene[3] (see Refs. 28 and 29 in Ref. 3). Therefore, because of the nonzero flexural rigidity in graphene, larger critical forces with respect to the predictions from elasticity theory, are to be expected.

Figure 4(b) shows the variation in $\langle h^2 \rangle$ versus ϵ_x for systems with $n_x=3,6,10$ when $n_y=3$. Vertical dashed line shows the transition points to the buckled state. Clearly the behavior of $\langle h^2 \rangle$ is the same for all cases. As we see, surprisingly, the buckling strain is independent of the longitudinal size [vertical dashed line in Fig. 4(b)] of GNRs and it varies in the range 0.84–0.89 % while for larger width, e.g., $n_y=4$, the buckling strain varies in the range 0.8–0.93 %. The average for $n_y=3$ is 0.8688% and for $n_y=4$ is 0.8677% which are very close. Therefore we conclude that the buckling strain is independent of the longitudinal dimension and depends only weakly on the width of the GNR.

It is important to note that higher ϵ_x (especially for the smaller system with small n_x) results in instabilities which makes the GNRs partially crumple (see Fig. 5). This is due to the sp^2 bond breaking at the nonuniform deformed (crumpled) region of edges. Red horizontal arrow in Fig. 4(b) indicates the instability point for $n_x=3$. To find the instabilities and the buckling thresholds, we calculated the variation in the boundary forces versus ϵ_x. The force on the left-hand side (LHS) edge is shown in Fig. 4(c). The forces on the LHS edge decrease to zero before the buckling thresholds which mean that GNRs at those points have an optimum length where the system does not feel any external forces [Fig. 5(a)]. We will return to this point later. In Fig. 4(c) the

TABLE II. The periodicity number (n) of the sine waves observed in the buckled laterally supported GNRs in the longitudinal direction versus the length of the GNR. The calculated buckling force from our MD calculations (f_c) and results from elasticity theory according to Eq. (6), f_{mn}, for two widths $n_y=3,4$. When calculating f_{mn} we used $h_0=0.1$ nm and $h_0=a_0$ was used for f'_{mn}. ϵ_c is the strain at which the GNR buckles.

n_y	$n_x\rightarrow$	2	3	4	5	6	7	8	9	10
3	n	3	4	5	7	9	11	11	14	14
	f_c	0.45	0.43	0.47	0.47	0.40	0.43	0.37	0.4	0.36
	f_{mn}	0.14	0.12	0.11	0.13	0.14	0.15	0.12	0.15	0.13
	f'_{mn}	0.40	0.34	0.31	0.36	0.40	0.42	0.35	0.42	0.36
	$\epsilon_c(\%)$	0.84	0.87	0.89	0.89	0.88	0.84	0.85	0.88	0.88
4	n	2	3	5	6	7	8	9	11	12
	f_c	0.38	0.37	0.34	0.33	0.32	0.34	0.32	0.32	0.32
	f_{mn}	0.07	0.07	0.09	0.09	0.08	0.08	0.08	0.09	0.09
	f'_{mn}	0.19	0.19	0.24	0.25	0.24	0.23	0.22	0.25	0.25
	$\epsilon_c(\%)$	0.90	0.93	0.93	0.91	0.87	0.89	0.87	0.8	0.80

vertical dashed line indicates the buckling threshold and the arrow gives the first sudden changes in the force (for three systems with $n_x=2,4,6$) which indicates an instability in the shape of the GNR.

As we mentioned above, Fig. 5 shows three snapshots of a GNR (having $n_x=2$ size) at three different strains. For Fig. 5(a) strain is $\epsilon=\epsilon_m$ (strain at optimum length). Two other snapshots are GNR before [Fig. 5(b)] and after [Fig. 5(c)] the first instability point in Figs. 4(b) and 4(c). The strain (and compression steps) in Fig. 5(c) is larger than in Fig. 5(b). Both strains in Figs. 5(b) and 5(c) are larger than the critical strain (ϵ_c). Brenner's potential is not responsible for the occurred nonhexagonal structures (bond-breaking effects) in some nonuniform deformed regions of Fig. 5(c). The reason is that in common covalent potentials, people use a drastic reduction in cutoff distance (here $\simeq 2$ Å) which has resulted in a good description of the material before fracture or bond breaking. But, it leads to an overestimation of critical loads and shear stresses in fracture mechanics and tribology, where bond breaking occurs.[15] Here we do not study the bond-breaking situation or fracture mechanism that can occur in GNRs by a continuous compression beyond the buckling state. Modification to Brenner's potential have been proposed in order to include fracture mechanisms and bond-breaking situations.[16] The idea to those modifications is to find nearest neighbors by a criterion other than distance[16] and this by employing empirical screening functions as introduced in Ref. 17.

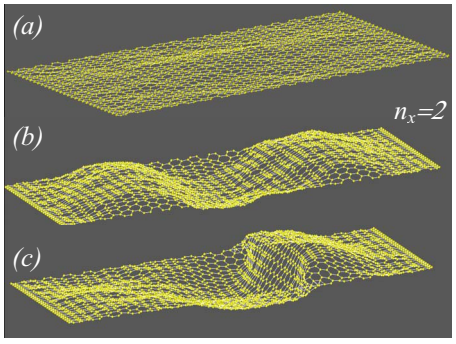

FIG. 5. (Color online) (a) GNR with $n_x=2$ size at its optimum length, (b) before, and (c) after the instability.

Static buckling deformations and the stability of buckled GNRs

In the last part of this paper, we calculate the change in the free energy of laterally supported GNRs subjected to axial strain. Due to the application of an external force on the boundary, an equilibrium approach is no longer applicable and a nonequilibrium MD is needed. Independent of the path and for a finite evolution rate, Jarzynski found an equality between the difference of the free energy and the total work done on the system (W) during a nonequilibrium evolution[7]

$$\Delta F = -\beta^{-1} \ln\langle \exp(-\beta W)\rangle, \tag{7}$$

where $\beta=1/k_BT$. The averaging is done over the realization of the switching process between the initial and the final states. Equation (7) makes a connection between the difference of the equilibrium free energy and the nonequilibrium work.

Using Eq. (7) we calculated the changes in the free energy when compressing the GNR of size $n_x=10$ and plot the results in Fig. 6(a). The inset shows the total work done on the system for ten simulations with different initial conditions. Comparing the curve for $\langle W\rangle$ and ΔF shows that the difference of the free energies are smaller than the total work which agree with $\langle W\rangle \geq \Delta F$ as can be derived from Eq. (7).[7] Figure 6(b) shows the change in W for systems having different values for n_x. The minimum in the free-energy curve corresponds to an equilibrium length, also to an amount of strain (ϵ_m) where there is zero force on the boundaries at $x=0$, $x=a$ [see Fig. 4(b)].

Notice that our noncompressed GNRs (in the beginning of the simulations) are flat honeycomb lattice structures which are not in a thermomechanically equilibrium state at finite temperature. Therefore the free energy of this state should be higher than the equilibrium state. It is well known that at finite temperature the equilibrium state of suspended graphene is not exactly a flat sheet and some intrinsic ripples

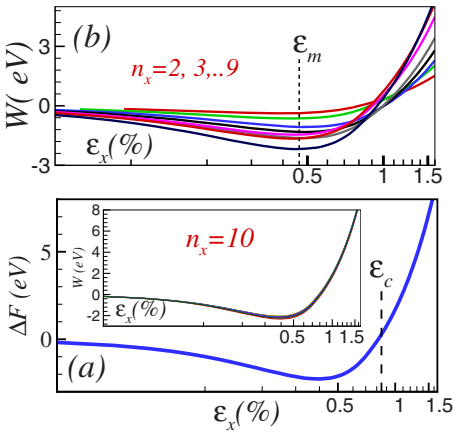

FIG. 6. (Color online) (a) Change in the free energy during compression for a system with size $n_x=10$ versus strain. The inset depicts the corresponding change in the total performed work on the system for ten simulations with different initial conditions. (b) Total work done on the system for various sizes versus strain.

are present.[12] At the optimum length our suspended GNRs are rippled [Fig. 5(a)] and the system is in the equilibrium state. Figure 6(a) shows the variation in the total free energy versus applied strain. As we see from Fig. 6(a) the rippled state (minimum point in free-energy curve) has a lower free energy with respect to the initial noncompressed GNRs, ($\Delta F=-2.27$ eV). The inset of Fig. 6(a) depicts the corresponding change in the total performed work on the system for ten simulations with different initial conditions. On the other hand, since the optimum length of the suspended GNR is less than the initial noncompressed length (a), we may conclude that at finite temperature the projected two-dimensional area $[a(1-\epsilon_m)\times b]$ of the GNR is less than the area of a flat GNR ($a\times b$). Surprisingly, as we see from Fig. 6(b) the boundary strain at the optimum length $\epsilon_m=0.48\%$ is size independent. The vertical dashed lines in Figs. 6(a) and 6(b) indicate the buckling strain, i.e., ϵ_c and the strain at the optimum length, i.e., ϵ_m, respectively. Free energy in the buckling point is less than the free energy of the initial noncompressed system but it is higher than the free energy for the rippled state (minimum value). Difference between the free energy of the rippled state and the buckled state is -1.87 eV. For the $n_x=10$ system we stopped the compression after the buckling threshold and equilibrated the system during a very long time and found static and stable sine wave deformations in the GNR.

IV. CONCLUSIONS

Deformations in the graphene nanoribbons subjected to axial boundary compression are static sine waves with different number of nodal lines, depending on the length of the GNRs. The deformations predicted from elasticity theory for the buckled rod and rectangular plate are similar to those obtained for the buckled GNRs in the case of free boundary condition and also for the laterally supported boundary condition. However, the critical force and flexural rigidity of GNRs are larger than predicted from elasticity theory. We found a linear relation for the stress-strain curve for small strains (i.e., before the buckling threshold). The buckling strain (0.86%) and the strain caused by the equilibrium length (0.48%) are independent of the longitudinal size of the system and they depend weakly on the width of GNRs. From the free energy of the GNRs at the buckling threshold, we found that they are thermodynamically more stable than those before compression, i.e., flat GNRs.

ACKNOWLEDGMENTS

This work was supported by the Flemish Science Foundation (FWO-Vl) and the Belgian Science Policy (IAP).

[1] C. Lee, X. Wei, J. W. Kysar, and J. Hone, Science **321**, 385 (2008).
[2] T. J. Booth, P. Blake, R. R. Nair, D. Jiang, E. W. Hill, U. Bangert, A. Bleloch, M. I. Gass, K. S. Novoselov, M. I. Katsnelson, and A. K. Geim, Nano Lett. **8**, 2442 (2008).
[3] G. Tsoukleri, J. Parthenios, K. Papagelis, R. Jalil, A. C. Ferrari, A. K. Geim, K. S. Novoselov, and C. Galiotis, Small **5**, 2397 (2009).
[4] V. M. Pereira, A. H. Castro Neto, and N. M. R. Peres, Phys. Rev. B **80**, 045401 (2009).
[5] B. I. Yakobson, C. J. Brabec, and J. Bernholc, Phys. Rev. Lett. **76**, 2511 (1996).
[6] H. Bu, Y. Chen, M. Zou, H. Yi, K. Bi, and Z. Ni, Phys. Lett. A **373**, 3359 (2009).
[7] C. Jarzynski, Phys. Rev. Lett. **78**, 2690 (1997).
[8] F. Colonna, J. H. Los, A. Fasolino, and E. J. Meijer, Phys. Rev. B **80**, 134103 (2009).
[9] D. W. Brenner, Phys. Rev. B **42**, 9458 (1990).
[10] R. M. Jones, *Buckling of Bars, Plates, and Shells* (Bull Ridge, Virginia, 2006), p. 50.
[11] J. H. Los, M. I. Katsnelson, O. V. Yazyev, K. V. Zakharchenko, and A. Fasolino, Phys. Rev. B **80**, 121405 (2009).
[12] A. Fasolino, J. H. Los, and M. I. Katsnelson, Nature Mater. **6**, 858 (2007).
[13] E. Cadelano, P. L. Palla, S. Giordano, and L. Colombo, Phys. Rev. Lett. **102**, 235502 (2009).
[14] K. Saitoh and H. Hayakawa, Phys. Rev. B **81**, 115447 (2010).
[15] M. Marder, Comput. Sci. Eng. **1**, 48 (1999).
[16] L. Pastewka, P. Pou, R. Pérez, P. Gumbsch, and M. Moseler, Phys. Rev. B **78**, 161402 (2008).
[17] M. I. Baskes, J. E. Angelo, and C. L. Bisson, Modell. Simul. Mater. Sci. Eng. **2**, 505 (1994).